www.czasopisma.pan.pl PAN POLSKA AKADEMIA NAUK www.journals.pan.pl

Arch. Metall. Mater. **68** (2023), 3, 1191-1204

DOI: https://doi.org/10.24425/amm.2023.145493

A. IŞIKGÜL[1*], H. AHLATCI[3], İ. ESEN[2], Y. TÜREN[3], O. YAĞIZ[3]

INVESTIGATION OF MECHANICAL PROPERTIES OF ACCELERATED COOLED AND SELF-TEMPERED H-TYPE STRUCTURAL SECTIONS

This study investigates mechanical properties of accelerated cooled and self-tempered (AC-ST) H-type S275JR quality steel sections in HEA120 and HEB120 sizes. The cooling process is conducted with a specially manufactured system that sprays a coolant consisting of a water + compressed air mixture on the section surfaces. Cooling times were applied as 10 and 30 seconds using 4 and 12 bar compressed air + water at an average constant pressure of 5 bar and a constant flow rate of 0.08 kg/s. In the HEA120 sections, the highest cooling rate was obtained with 83°C/s in the web region under the cooling time of 30 s and the air pressure cooling condition of 12 bar. At the cooling rate up to 6°C/s, the microstructure is transformed to acicular ferrite and polygonal ferrite phase from Ferrite+Pearlite. But upper bainite phase was formed at a cooling rate of 30°C/s, and a small amount of martensite and lower bainite microstructures were observed at a cooling rate of 60°C/s and above. The hardness in the untreated sections, in the range of 106-120 HB, was increased to 195 HB at a cooling rate of 83 C/s in the web region of the HEA120 section. For a cooling rate of 23°C/s, the maximum compressive residual stresses of –352 MPa are measured in the crotch region of the HEB120. And for a cooling rate of 6°C/s, the maximum tensile residual stresses of 442 MPa were determined in the flange region of the HEA120 section.

Keywords: H-Type Sections; Accelerated Cooling and Self-Tempering (AC-ST); Construction Steel; Cooling Rate

1. Introduction

The Accelerated Cooling and Self-Tempering (AC-ST) has become popular in improving material strength and the "QST-Quenching and Self-Tempering" unit has been in operation for 30 years [1,2] However, while there are studies with water in the literature [3-5], the cooling process with the water+air mixture applied in this study has not been found. H section European lightweight wide flange (HEA) and H section European standard wide flange (HEB) sections with S275JR commercial quality steel are used commonly for construction such as buildings, suspension bridges, tunnels, etc. [6]. The production of the high-strength structural steels requires high technology and precision manufacturing processes. It is also a critical issue that these products undergo a very strict quality control inspection before they are used in buildings. For this reason, the industry continues to improve and produce new high quality building components [7-9]. In particular, the thermomechanical process allows the material properties that were previously thought to be opposite to be provided together [10,11]. At the same time, high yield strength and high toughness can be added to the material together with this process, and its ability to be combined with welding can be preserved. Based on this, ArcelorMittal Differdange introduced the patented HISTAR quality to the market by using the QST unit in the heavy section rolling line and developed together with the Center de Recherches Métallurgiques (CRM) in Liège [1,3,12,13].

The QST process can be considered an extension of the thermo-mechanical process and is therefore classified as a thermo-mechanically controlled process. The QST unit is found after the rolling mill. While all surfaces of the section coming out from here are cooled with water in the given QST unit, the cooling process is stopped before it reaches the inner core. When the temperature equalizes in the section, the outer layers are tempered by the heat flow from the core to the surface. Thus, with this process, it is possible to manufacture even the heaviest steel wide flange sections from high-strength steels [2,4,6,13-16].

It is expected that the steels will have a bainite (similar) microstructure with both high strength and high toughness due to the fine grained Ferritic+Pearlitic microstructures of the steels

[1] KARABÜK IRON STEEL INDUSTRY TRADE AND CO. INC., RESEARCH AND DEVELOPMENT DEPARTMENT, KARABÜK, TURKEY
[2] KARABÜK UNIVERSITY, DEPARTMENT OF MECHANICAL ENGINEERING, KARABÜK, TURKEY
[3] KARABÜK UNIVERSITY, DEPARTMENT OF METALLURGY AND MATERIALS ENGINEERING, KARABÜK, TURKEY

* Corresponding author: aisikgul@kardemir.com

during the AC-ST heat treatment phase after being brought to the austenite phase under a protective atmosphere to be applied to the sections [7,17]. The transformation of the austenite phase into martensite phase by quenching in steels creates high residual stresses caused by non-uniform volumetric changes [18].

Until now, high-flow water spraying process is widely used in QST units, and there is limited information about operating parameters. In addition, cooling systems in which water and air are used together have not been found in the literature. Therefore, conducting research on the use of the water+air mixing systems will provide less water consumption and will be an alternative to QST units. Within the scope of the study, microstructure, hardness and residual stress of the HEA120 and HEB120 S275JR quality steel sections are investigated by applying AC-ST process under versus different cooling time and air pressure.

2. Materials and Methods

In this study, steel sections with dimensions of the HEA120 and HEB120 manufactured by hot rolling of the S275JR grade steel beam blank with 280×360 mm cross-section were used. The section properties of the studied construction steels are presented in TABLE 1. The chemical compositions of the HEA120 and HEB120 type S275JR quality structural steel used in the study are given in TABLE 2. In TABLE 2, the abbreviation C_{EV} stands for carbon equivalent. The chemical composition of the tested materials was determined by measuring with an optical emission spectrometer according to the ASTM E 415 method.

The method applied in this study is summarized in Fig. 1. Accordingly, Fig. 1a represents the annealing, Fig. 1b represents the AC-ST and Fig. 1c represents the characterization processes. This system consists of the necessary nozzles that pulverize the water+air mixture, plates, and main chassis. Air pressure and cooling time parameters are adjusted in the range of 4 and 12 bar and 10 and 30 s on the system. Microstructure, hardness, and residual stress tests of the AC-ST heat-treated sections were conducted.

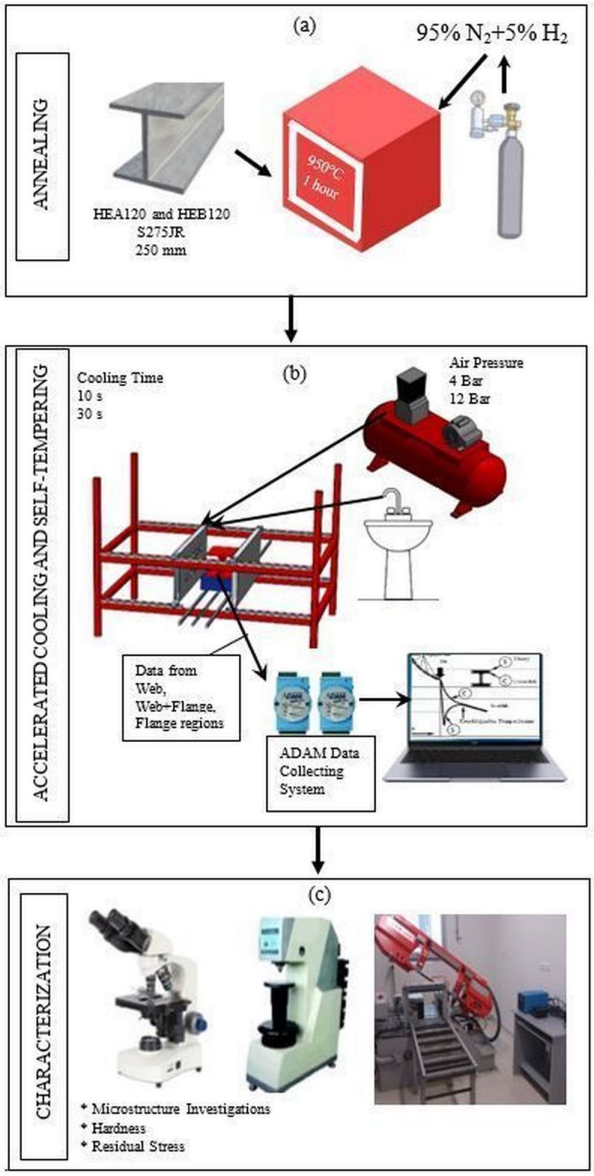

Fig. 1. Experimental flow diagram for a) annealing heat treatment, b) AC-ST process and c) characterization of the HEA120 and HEB120 sections

TABLE 1

Properties of the sections

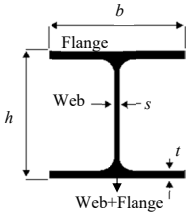

Dimensions (mm)	h	b	s	t	Unit mass (kg/m)
HEA120	114	120	5	8	19.9
HEB120	120	120	6.5	11	26.7

TABLE 2

Chemical compositions

Material Size and Quality		(%wt)								Ppm
		C	Mn	S	P	Cu	V	Nb	C_{EV}	N
Standard	EN 10025-2 (max)	0.24	1.60	0.045	0.045	0.55	0.15	0.06	0.40	120
Measured Results	HEA120 (S275JR)	0.094	0.756	0.015	0.0125	0.063	0.0024	0.0002	0.239	68
	HEB120 (S275JR)	0.101	0.718	0.023	0.0164	0.047	0.0009	0.0002	0.234	58

In the AC-ST process, K-type thermocouples on the web, web+flange and flange of the HEA120 and HEB120 type sections cut in 250 mm length were placed and cooling diagrams were obtained with the help of ADAM software. The austenitization annealing process of the sections was carried out for 1 hour [19,20] at 950°C under 95%N_2+5%H_2 atmosphere [21] in furnace with Telmika model temperature control unit.

In the study, AC-ST heat treatment was applied to 2 different section types (HEA120 and HEB120) at 4 and 12 bar air pressure with a cooling time for 10 and 30 s (Fig. 2). While applying AC-ST heat treatment, the distance between the cooling plate where the nozzles are located, and the section is set to 60 mm.

Fig. 2. Photograph of the AC-ST process

For the microstructural analysis of the examined sections, samples from the web, web+flange and flange regions were cut and mounted in bakelite (thermosetting plastic) molds with a hot mounting machine. The samples were sanded down to 2500 size paper and polished in an automatic polisher using felts up to 1 μm. Prepared samples were etched with 3% Nital solution for 3 s. Images were obtained using light microscopy at ×500 magnification.

The hardness of the sections was measured in the OPTOBUL brand Brinell hardness device with 5 mm balls and under 0.75 kgf. Hardness values were determined based on the average of at least five measurements taken from the section surfaces corresponding to the web, web+flange and flange regions.

Residual stress measurement was made by cutting (sectioning) method, which is a destructive residual stress measurement method. A total of 2 measurements per section were made by attaching 1 strain gauge to the web and flange regions of each section. These measurements were applied to 5 different sections in total according to cooling conditions and section types (untreated, HEA120 4 bar 10 s, HEA120 4 bar 30 s, HEA120 12 bar 30 s and HEB120 4 bar 10 s). The strain gauges used are 5 mm in size, 350-ohm electrical resistance and are of the type that can measure in a single axis. Strain gauges with cables were attached to the web and flange region after cleaning the surface before residual stress measurements in the sections, and Micro Measurement VPG brand (Vishay) CEA-06240-UZ-120 model was attached to the device with the sockets at the cable end to collect data. Time-dependent strain measurements were made by making two cuts under the water-cooled band saw, leaving a distance of 10 mm before and after the strain gauges placed on the examined sections (Fig. 3). Then, by applying Hooke's law to strain values obtained from the device, compressive or tensile residual stress values were determined.

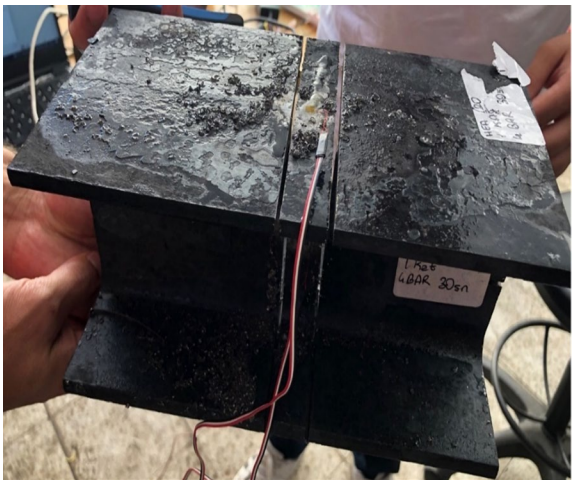

Fig. 3. Section with cutting method applied

3. Results and Discussion

Cooling graphs of the investigated AC-ST sections with respect to time are given in Fig. 4. It was determined that the finish cooling temperature (FCT) in the web region of the AC-ST HEA120 section decreased to around 240°C for 4 bar 10 s (Fig. 4a), while this value obtained a decrease in around 30°C for both 4 bar 30 s (Fig. 4c) and 12 bar 30 s (Fig. 4e). After the FCT point, an increase in the temperature on the web region of the AC-ST HEA120 section due to self-tempering with the effect of the residual temperature in the section centre obtained up to 400°C for 4 bar 10 s (Fig. 4a), 200°C for 4 bar 30 s (Fig. 4c) and 150°C for 12 bar 30 s (Fig. 4e). FCT of the web+flange of the AC-ST HEA120 section was not observed for 10 and 30 s under 4 bar pressure (Fig. 4a and 4c) except for 12 bar 30 s (Fig. 4e). While the cooling curve of the web+flange region decreased to 450°C with the time increased under 4 bar pressure, the cooling curve under 12 bar pressure decreased rapidly up to 150°C and then self-tempered up to 300°C. When the cooling curves in the flange regions of the AC-ST HEA120 sections are examined, an initial rapid and then a stable state decrease in the cooling curve was observed with increasing cooling time and increasing air pressure. However, self-tempering did not occur in the flange region. Although the cooling curves for the AC-ST HEB120 section are like the AC-ST HEA120 section, the difference between the temperature values of the web+flange and flange regions is approximately 100°C higher as the pressure and cooling time increase due to the higher wall thickness of the AC-ST HEB120

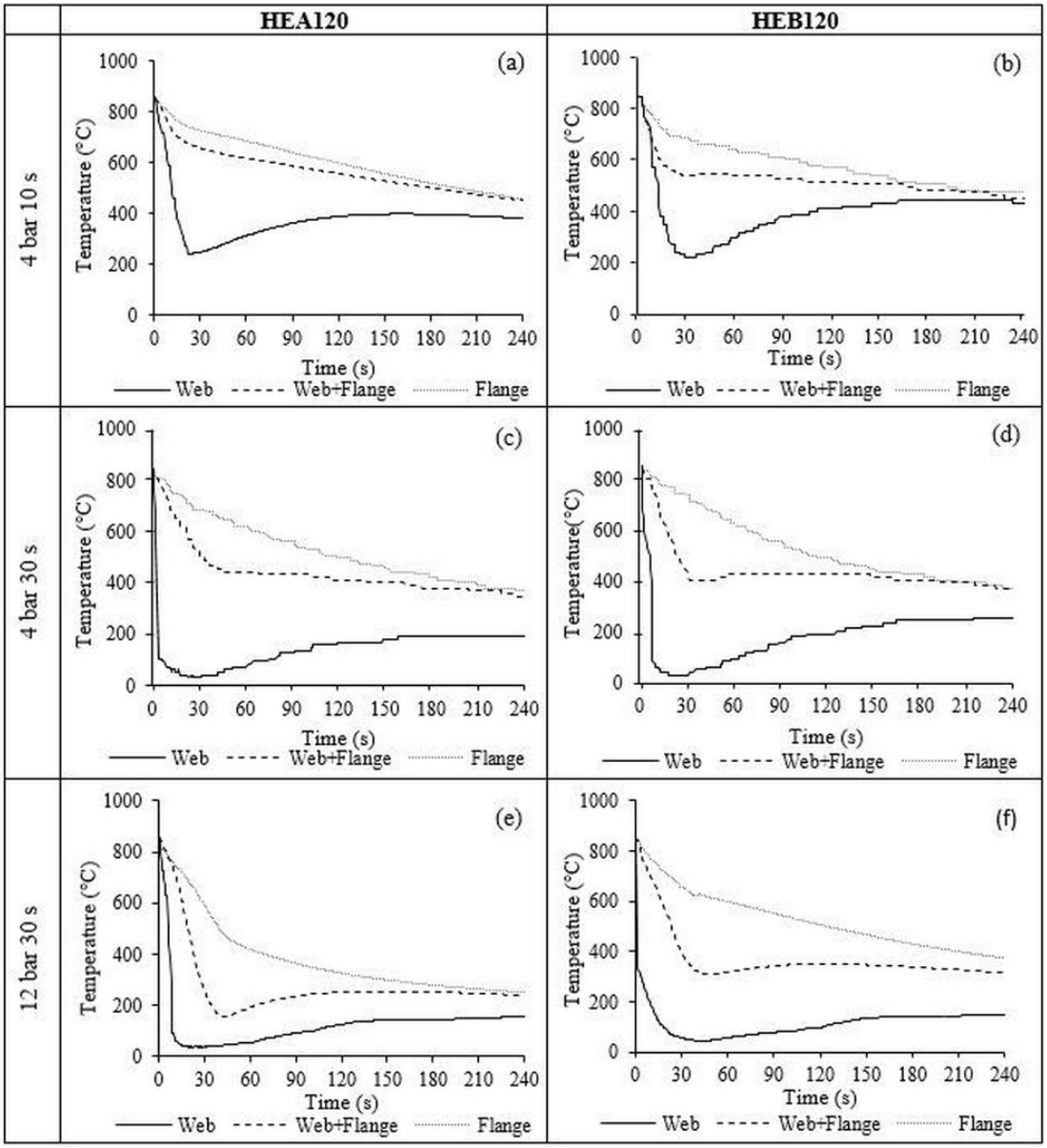

Fig. 4. Temperature versus time in the web, web+flange and flange regions of the a) AC-ST HEA 120 section at 4 bars for 10 seconds, b) AC-ST HEB 120 section at 4 bars for 10 seconds, c) AC-ST HEA 120 section at 4 bars for 30 seconds, d) AC-ST HEB 120 section at 4 bars for 30 seconds, e) AC-ST HEA 120 section at 12 bars for 30 seconds, f) AC-ST HEB 120 section at 12 bars for 30 seconds

section. It was observed that the self-tempering process takes place in the web and web+flange region of the AC-ST HEB120 section.

The cooling rates of the AC-ST applied HEA120 and HEB120 section determined by measuring the slopes of the cooling curves (Fig. 4) were displayed in Fig. 5. In addition, the highest cooling rate was found in the web region of the HEA120 section under 12 bar 30 s as 83°C/s. The cooling rates in the web+flange and flange regions were assumed as low cooling rates varying in the range of 4-23°C/s. The reason for the high cooling rate in the web region is thought to be due to the water+air mixed nozzle position (Fig. 2) directly seeing the web region.

Considering the cooling rates in Fig. 5, it is observed that the cooling rates of the HEA120 section were higher than that of the HEB120 section because of its thinner wall thickness (Fig. 6). As the thickness of the sections increases, the cooling rate decreases logarithmically independent of time and pressure, and the range of variation narrows. The logarithmic variation of the cooling rate depending on the thickness is given in Eq. (1).

$$C_R = \exp[(T - 14.628)/-2.217] \quad (1)$$

Where T is the wall thickness and C_R is cooling rate.

In both HEA120 and HEB120 sections applied AC-ST, the cooling rate increases with the increase for air pressure and cooling time. Since the cooling system installed in this study is directly parallel to the web, the cooling in the web region is effective with exposure time. A significant effect of the water+air pressure, on the other hand, is seen on the cooling of the flange area.

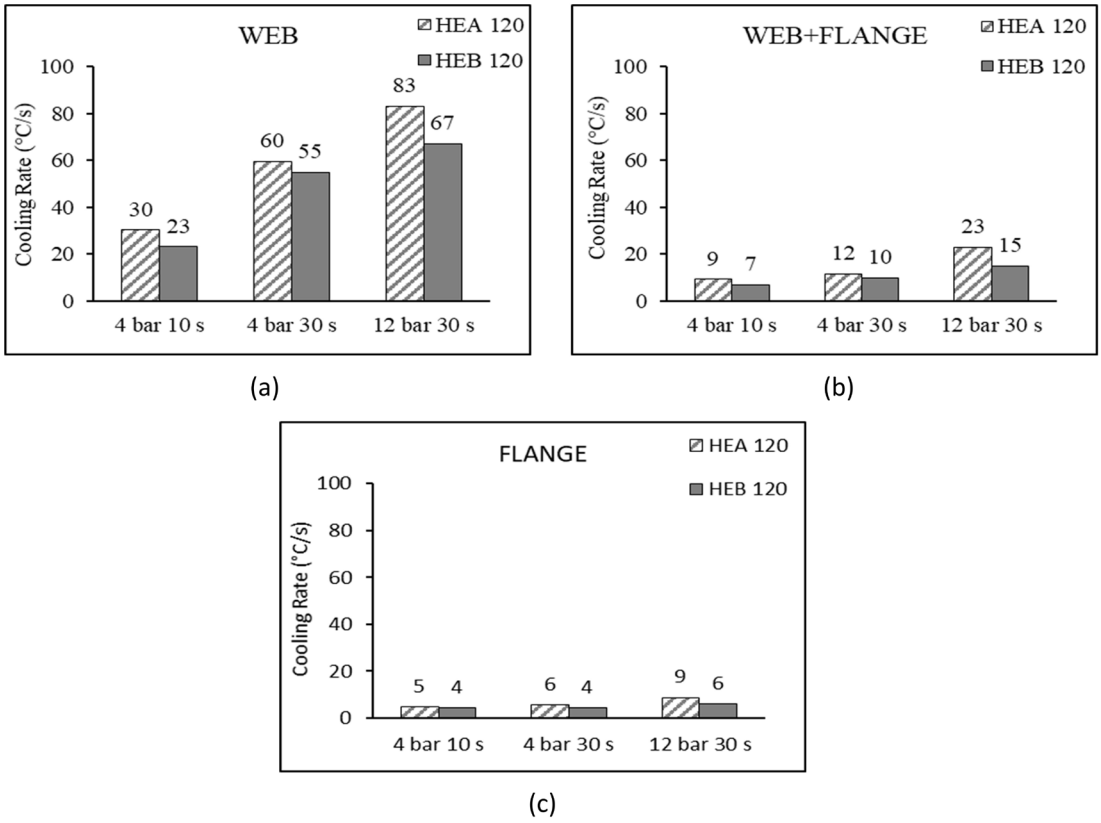

Fig. 5. Variation of the cooling of different regions of the AC-ST HEA120 and HEB120 sections for different parameters (pressure and cooling time). a) web, b) web+flange and c) flange regions

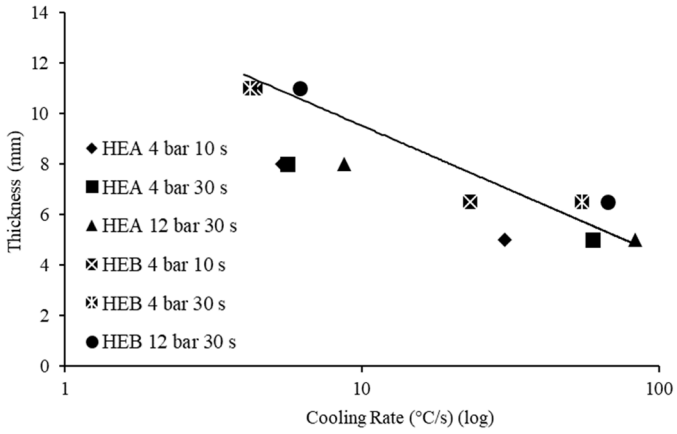

Fig. 6. Thickness versus cooling rate in the web, web+flange and flange regions of the AC-ST HEA120 and HEB120 sections for different parameters (pressure and cooling time)

3.1. Microstructure

Microstructure images taken at ×500 magnification from web, web+flange and flange regions on the cross-sectional surface of the HEA120 and HEB120 sections with and without AC-ST heat treatment are given in Fig. 7 and 8, respectively. The microstructures of the untreated sections are Ferrite+Pearlite (Fig. 7a-c and Fig. 8a-c).

The light microscopy images (Fig. 7 and 8) of the web region of the AC-ST HEA120 and HEB120 sections with high cooling rate showed that the Ferrite+Pearlite phases turned into acicular and/or polygonal and lath and/or thin lamella-like phases. While the microstructure of the flange regions with a low cooling rate consists of granular and/or polygonal and/or lamellar microstructures. In the studied low carbon (up to 0.1wt.%) steels, sufficient hardenability can only be achieved using the accelerated cooling by martensitic transformation. However, it is thought that bainite, sorbite and acicular ferrite consisting of hairy and/or elongated cementite microstructures are formed by the diffusion of carbon from martensite supersaturated with carbon due to the self-tempering after accelerated cooling [22-24].

These phases formed in steels can be difficult to detect with a conventional light microscope. Therefore, the SEM images with EDS map analysis are presented in Fig. 9-12 for exhaustive inspections of the morphology and characteristics of the different phases in the AC-ST sections.

SEM images-EDS map analysis of the web regions of the AC-ST HEA120 sections for 12 bar 30 s are presented in Fig. 9 and 10. Fig. 9a shows the SEM images with 5 kX magnification while Fig. 9b displays 15 kX magnification view of the region marked by the rectangle on Fig. 9a. Fig. 9c presents the EDS map analysis of the region marked with circle (k) on the image on Fig. 9b. Fig. 9d represents the map data analyses results for Fe (red colour) and C (green colour) in Fig. 9c. Moreover, another SEM image of the same sample is presented in Fig. 10a. And Fig. 10b display the EDS map analyses of the region marked with

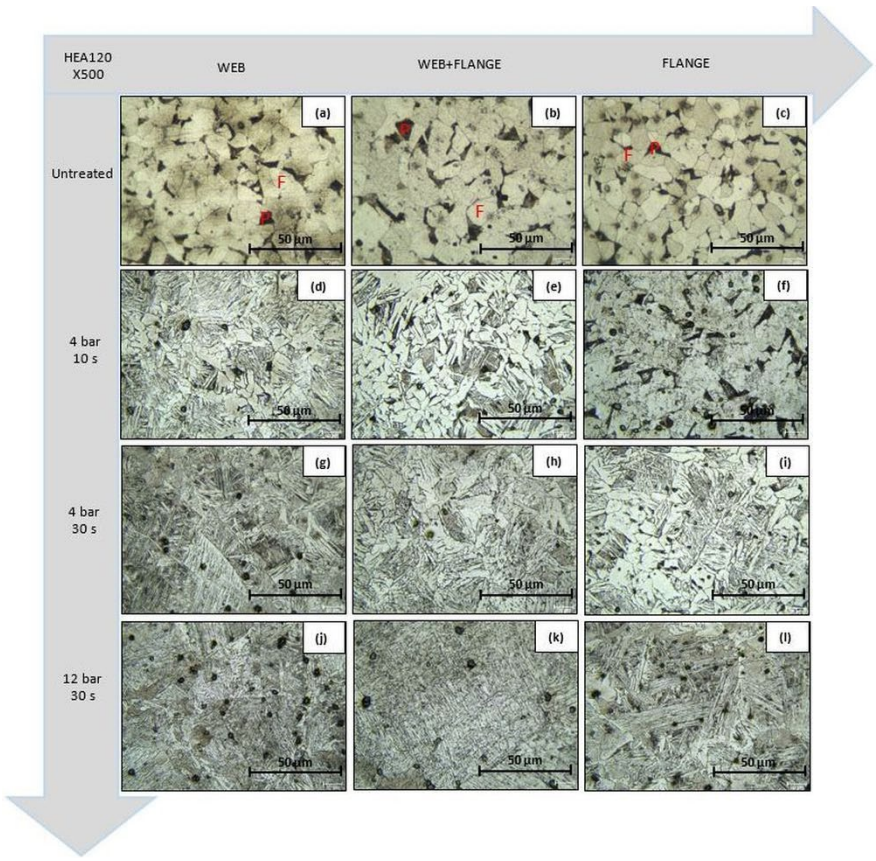

Fig. 7. ×500 magnification cross-sectional images in the web, web+flange and flange regions of the AC-ST HEA120 sections for different parameters (pressure and cooling time). Abbreviations: F: Ferrite, P: Pearlite

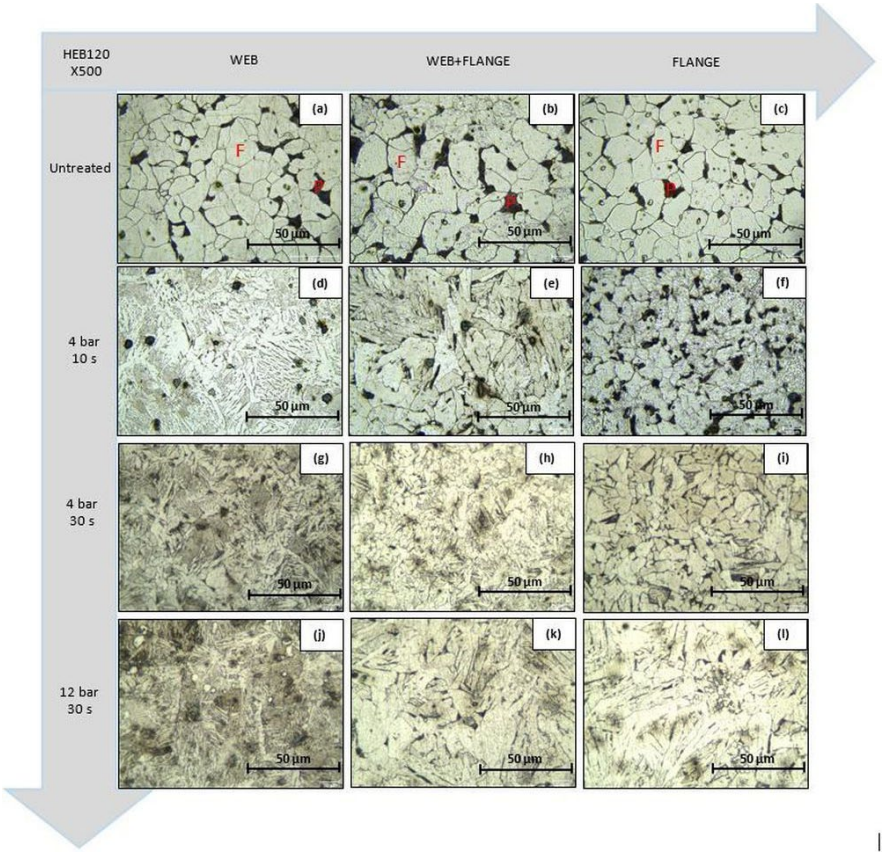

Fig. 8. ×500 magnification cross-sectional images in the web, web+flange and flange regions of the AC-ST HEB120 sections for different parameters (pressure and cooling time). Abbreviations: F: Ferrite, P: Pearlite

(m) in Fig. 10a. Fig. 10c represent the map data analyses results for Fe (red colour) and C (green colour) in Fig. 10b. Fig. 10d represents the EDS map analysis of the region marked with (n) in Fig. 10a. Fig. 10e represent the map data analyses results for Fe (red colour) and C (green colour) in Fig. 10d. The EDS map analysis result given in Fig. 9c proves the formation of lower bainite and/or small amount of martensite (LB/M) at a cooling rate of 83°C/s. In Fig. 10b, sorbite and/or upper bainite phases (S/UB) are seen, while in Fig. 10c acicular ferrite and/or polygonal ferrite (AF/PF) phases are detected.

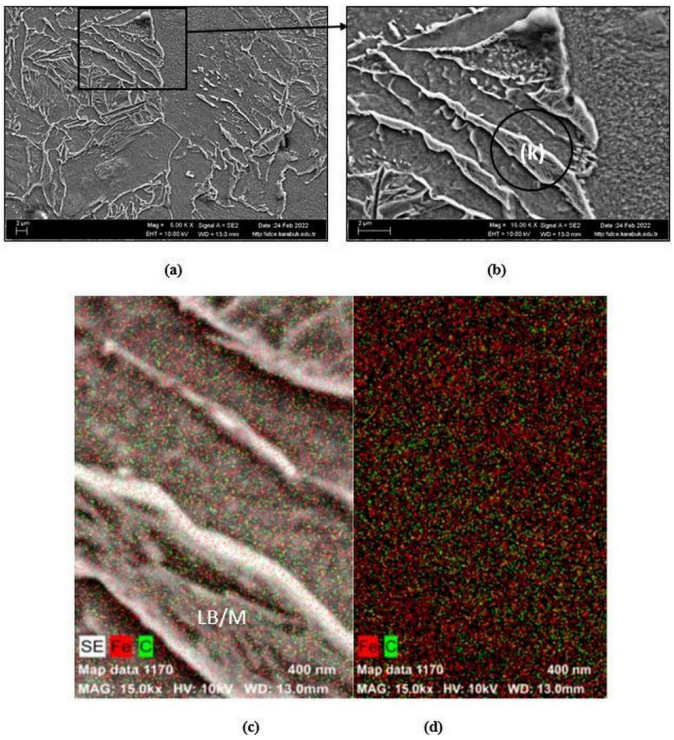

Fig. 9. SEM images of the web region of the AC-ST HEA120 section with 12 bar 30 s. Here, LB/M: lower bainite and/or small amount of martensite denote the microstructure types. a) 5 kX magnification image, b) 15 kX magnification image marked with a rectangle in a. Images with captions c) represent elemental map analyses of the area marked with (k) in b. d) represent the map data analyses results for Fe (red colour) and C (green colour) in c. Cooling rate is 83°C/s

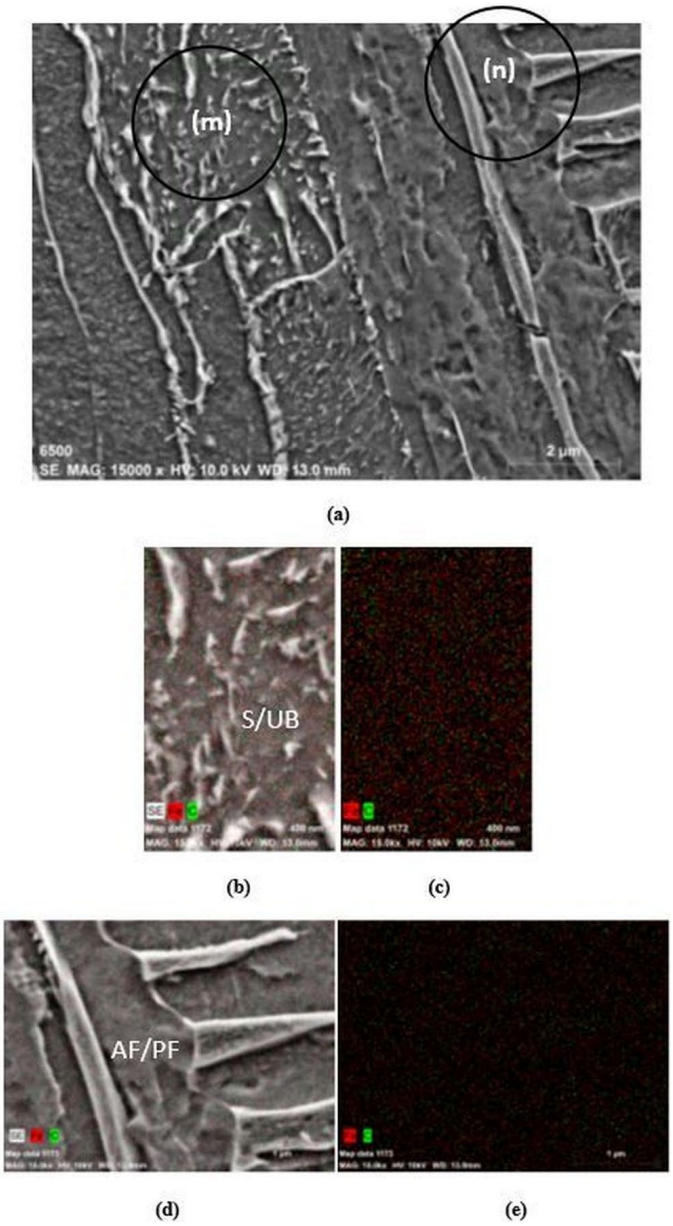

Fig. 10. SEM images of the web region of the AC-ST HEA120 section with 12 bar 30 s. Here, AF/PF: acicular ferrite and/or polygonal ferrite and S/UB: sorbite and/or upper bainite denote the microstructure types. a) 15 kX magnification image. Images with captions b) represent elemental map analyses of the area marked with circles in a. c) represent the map data analyses results for Fe (red colour) and C (green colour) in b. Images with captions d) represent elemental map analyses of the area marked with circles in a. e) represent the map data analyses results for Fe (red colour) and C (green colour) in d

Das et. al. examined the effect of cooling rate on microstructure of Pressure Vessel Steel and found that the microstructure was both ferrite and bainite for cooling rates of 0.15 to 0.3°C/s, only bainite for 1 and 2°C/s cooling rate, both bainite and martensite for cooling rate of 5-15°C/s, while full martensitic transformation was observed for cooling rates of 20°C/s and above [25]. Rasouli et. al. reported that as-received ferritic-pearlitic microstructure of a commercial micro alloyed forging steel can be changed into the acicular ferrite, bainite and/or martensite by increasing the cooling rate. By deformation at 1150°C and cooling rate of 3°C/s acicular ferrite microstructure is produced. Increasing the cooling rate to 7 and 15°C/s produces the bainite and martensite microstructures [26]. Unlike the studies [25,26] above, acicular ferrite and upper bainite phases were formed up to a cooling rate of 23°C/s, and small amount of martensite phase was not observed in the microstructure. However, at high cooling rates above 23°C/s, acicular ferrite, upper and/or lower (U/L) bainite and tiny amounts of martensite (Fig. 9c, 10b and 10d) can be observed. This can be attributed to the low carbon (0.1wt.%C and 0.7wt.% Mn) content of the HEA120 and HEB120 sections examined in this study, compared to the material of Das et. al. (0.2wt.%C and 1.38wt.%Mn).

SEM images-EDS map analysis of the web+flange region of the AC-ST HEA120 sections for 12 bar 30 s are presented in Fig. 11. Fig. 11a shows the SEM images with 5 kX magnifica-

tion while Fig. 11b displays 15 kX magnification view of the region marked by the rectangle on Fig. 11a. Fig. 11c and 11e present the EDS map analysis of the regions marked with a circle on the image on Fig. 11b. Fig. 11d and 11f represent the map data analyses results for Fe (red colour) and C (green colour) in Fig. 11d and 11e respectively. The EDS map analyse results given in Fig. 11c proves the formation of sorbite and/or upper bainite (S/UB) and in Fig. 11e acicular ferrite and polygonal ferrite (AF/PF) are seen at a cooling rate of 23°C/s.

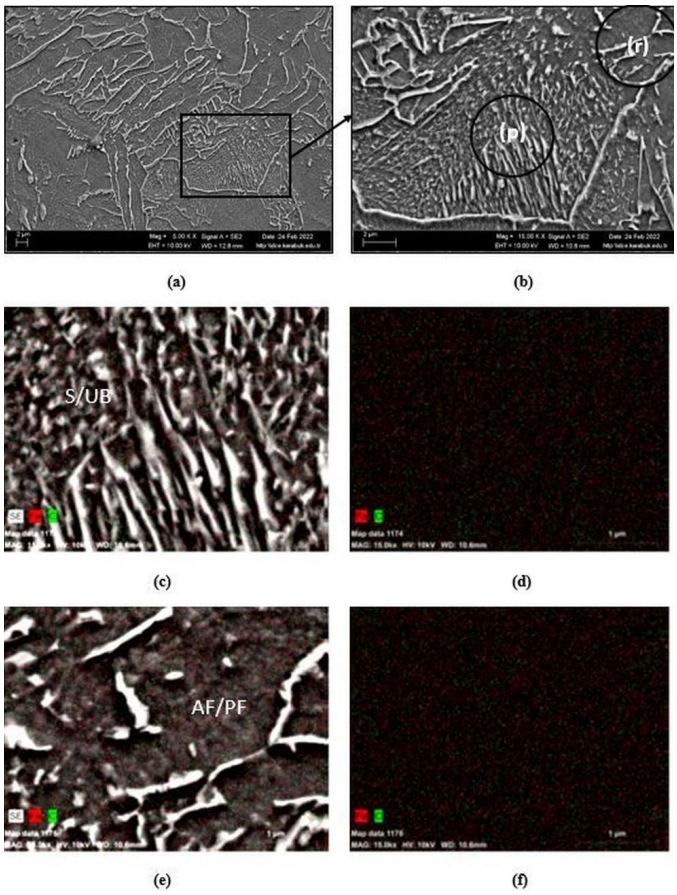

Fig. 11. SEM images of the web+flange region of the AC-ST HEA120 section with 12 bar 30 s. Here S/UB: sorbite and/or upper bainite, UB: upper bainite denote the microstructure types. a) 5 kX magnification image, b) 15 kX magnification image marked with a rectangle in a. Images with captions c) represent elemental map analyses of the area marked with circles (p) and (r) in b. d) represent the map data analyses results for Fe (red colour) and C (green colour) in c. Images with captions e represent elemental map analyses of the area marked with circles (p) and (r) in b. f) represent the map data analyses results for Fe (red colour) and C (green colour) in e. Cooling rate is 23°C/s

It is thought that sorbite formation occurs [27-29] because of the slower cooling rate (23°C/s), FCT to 200°C and ST to above 300°C. Bainite occupies a region between fine pearlite and/or sorbite and martensite phases in a temperature range where self-diffusion is limited but there is insufficient driving force to form martensite. Bainite forms when steel is cooled slower than the rate required to form martensite but faster than the rate that would be required to form pearlite. Upper bainite is obtained by transformation at a higher temperature. In upper bainite, cementite is precipitated between ferrite platelets. In lower bainite, some cementite is precipitated between lamellar ferrites as seen in the web+flange region of the AC-ST HEA120 sections for 12 bar 30 s (Fig. 11c) [30-33]

The SEM images-EDS map analysis of the flange region of the AC-ST HEA120 sections for 12 bar 30 s are presented in Fig. 12. Here, Fig. 12a depicts the SEM images with 5 kX magnification while Fig. 12b displays 15 kX magnification view of the region marked by the rectangle on Fig. 12a. And Fig. 12c, 12e and 12g represent the EDS map analysis of the regions marked with a circle on the image in Fig. 12b. Fig. 12d, 12f, 12h represent the map data analyses results for Fe (red colour) and C (green colour) in Fig. 12c, 12e and 12g respectively. The sign AF/PF denotes acicular ferrite and/or polygonal ferrite in

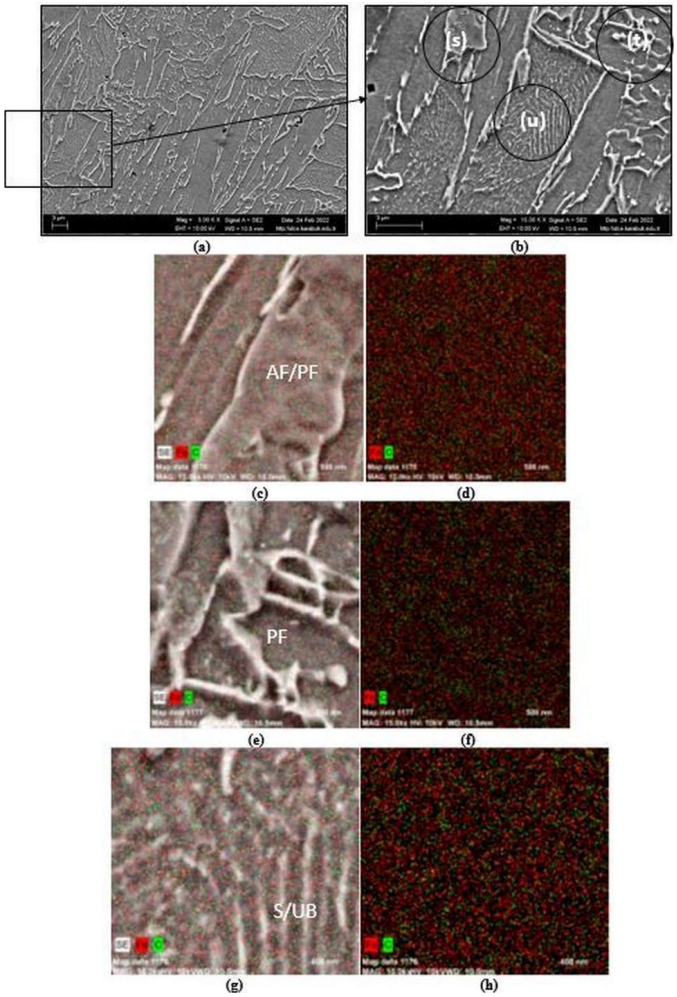

Fig. 12. SEM images of the flange region of the AC-ST HEA120 section with 12 bar 30 s. Here, AF/PF: acicular ferrite and/or polygonal ferrite and S/UB: sorbite and/or upper bainite denote the microstructure types. a) 5 kX magnification image, b) 15 kX magnification image marked with a rectangle in a. Images with captions c represent elemental map analyses of the area marked with circles (s), (t) and (u) in b. d) represent the map data analyses results for Fe (red colour) and C (green colour) in c. Images with captions e represent elemental map analyses of the area marked with circles (s), (t) and (u) in b. f) represent the map data analyses results for Fe (red colour) and C (green colour) in e. Images with captions g) represent elemental map analyses of the area marked with circles (s), (t) and (u) in b. h) represent the map data analyses results for Fe (red colour) and C (green colour) in g. Cooling rate is 9°C/s

12c and 12e. And the symbol S/UB in 12e represent the sorbite and/or upper bainite phases. The cooling rate in this experiment is calculated as 9°C/s. Due to the low cooling rate of 9°C/s compared to other high cooling rates, sorbite and/or upper bainite phases are formed more in the microstructure. Even the sorbite phase tends to transform into the fine pearlite.

LB/M and S/UB phases are detected in Fig. 13 with the cooling rates 60°C/s and these phases similar to do the phases formed in Fig. 9 and 10 with the cooling rates 83°C/s. S/UB sorbite and/or upper bainite phases were formed in the region indicated by (y) in Fig. 13b, and LB/M lower bainite and/or small amount of martensite phases were formed in the region indicated by (z). Fig. 13d and 13f represent the map data analyses results for Fe (red colour) and C (green colour) in Fig. 13c and 13e respectively.

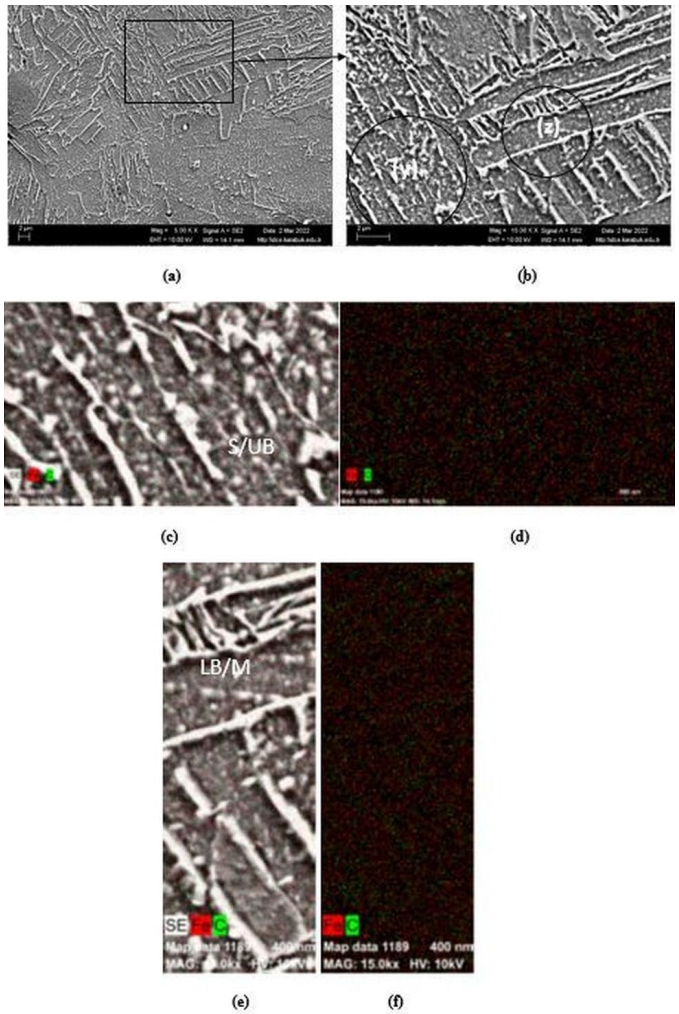

Fig. 13. SEM images of the web region of the AC-ST HEA120 section with 4 bar 30 s. Here, LB/M: lower bainite and/or small amount of martensite and S/UB: sorbite and/or upper bainite denote the microstructure types. a) 5 kX magnification image, b) 15 kX magnification image marked with a rectangle in a. Images with captions c represent elemental map analyses of the area marked with circles (y) and (z) in b. d) represent the map data analyses results for Fe (red colour) and C (green colour) in c. Images with captions e) represent elemental map analyses of the area marked with circles (y) and (z) in b. f) represent the map data analyses results for Fe (red colour) and C (green colour) in e. Cooling rate is 60°C/s

SEM representation of the AC-ST HEA120 sections at 30°C/s cooling rate is given in Fig. 14a. SEM analysis showed sorbite and/or upper bainite (S/UB) and acicular ferrite and/or polygonal ferrite (AF/PF) phases. Here, Fig. 14b represents the elemental map analyses of the area marked with circle (x) in Fig. 14a and Fig. 14c represent the map data analyses results for Fe (red colour) and C (green colour) in Fig. 14b.

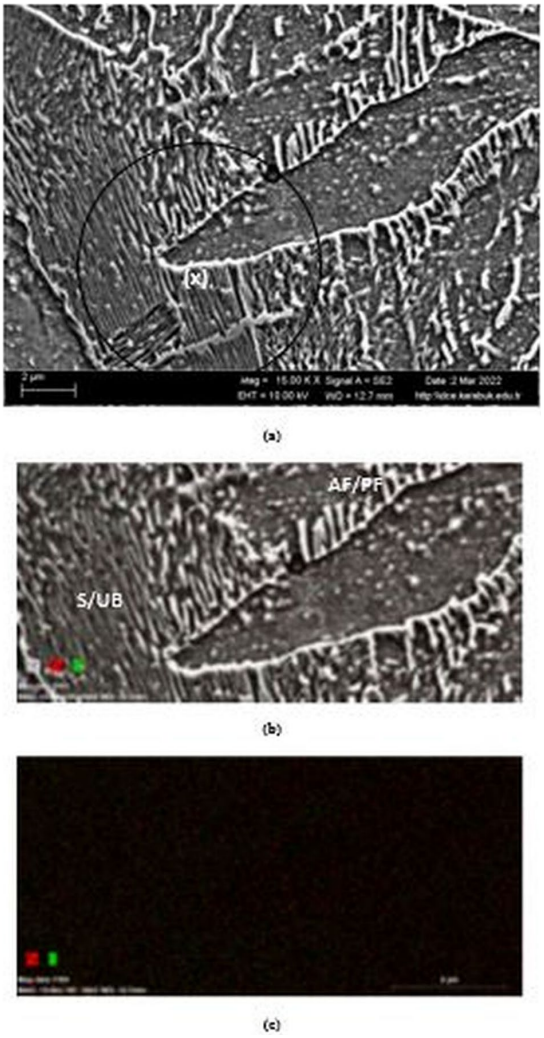

Fig. 14. SEM images of the web region of the AC-ST HEA120 section with 4 bar 10 s. Here, S/UB: sorbite and/or upper bainite, AF/PF: acicular ferrite and/or polygonal ferrite denote the microstructure types. a) 15 kX magnification image. Image with caption b) represents elemental map analyses of the area marked with circle (x) in a. c) represent the map data analyses results for Fe (red colour) and C (green colour) in b

In the SEM images of the flange region where the cooling rate is the lowest (4°C/s) in Fig. 15, AF: acicular ferrite in the white regions and PF: polygonal ferrite phases in the grey regions were observed. Here, Fig. 15b represents the elemental map analyses of the area marked with circle (w) in Fig. 15a and Fig. 15c represent the map data analyses results for Fe (red colour) and C (green colour) in Fig. 15b.

The summary results of the SEM examinations of the AC-ST HEA120 section using web, web+flange and flange regions in different parameters are given in TABLE 3.

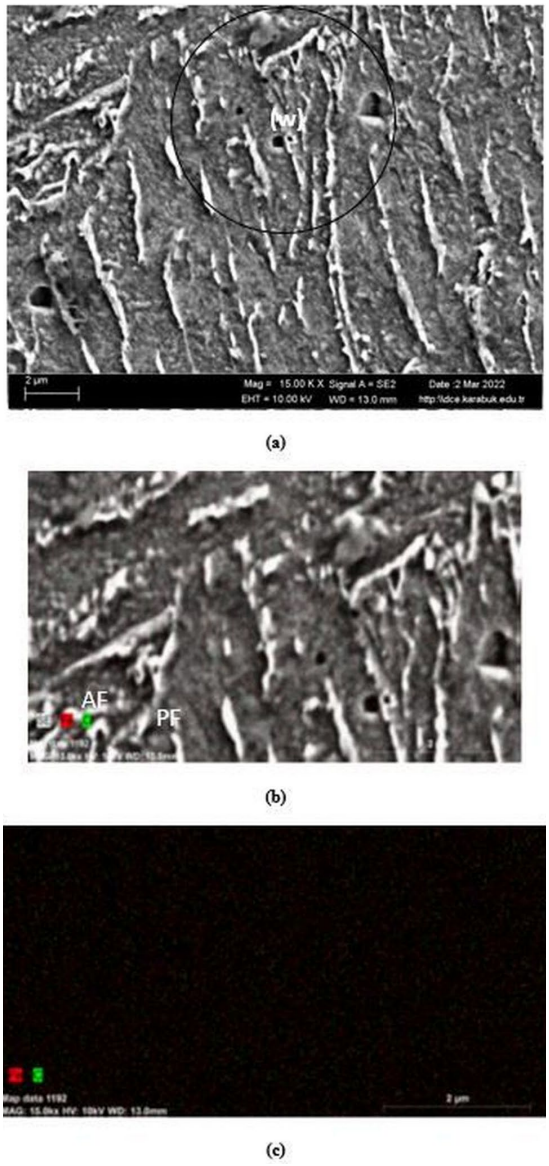

(a)

(b)

(c)

Fig. 15. SEM images of the flange region of the AC-ST HEA120 section with 4 bar 10 s. Here, AF: acicular ferrite, PF: polygonal ferrite denotes the microstructure types. a) 15 kX magnification image. Image with caption b) represents elemental map analyses of the area marked with circle (w) in a. c) represent the map data analyses results for Fe (red colour) and C (green colour) in b. Cooling rate is 4°C/s

TABLE 3

Microstructures* obtained after AC-ST heat treatment

Cooling Condition	Cooling Rate (°C/s)			Microstructure		
	Web	Web +Flange	Flange	Web	Web +Flange	Flange
12 bar 30 s	83	23	9	LB/M	S/UB	S/UB
				S/UB	AF/PF	AF/PF
				AF/PF		PF
4 bar 30 s	60	12	6	LB/M	S/UB	AF
				S/UB	AF/PF	PF
4 bar 10 s	30	9	4	S/UB	S/UB	AF
				AF/PF	AF/PF	PF

* Abbreviations: LB/M: lower bainite and/or small amount of martensite, S/UB: sorbite and/or upper bainite, AF/PF: acicular ferrite and/or polygonal ferrite.

3.2. Hardness

The hardness results obtained from the web, web+flange and flange regions of the sections of the AC-ST applied sections at different cooling parameters are given in Fig. 16. When the results were examined, it was decided that the web region hardness values of the AC-ST sections were higher than the other regions. After that, the stiffness of the web+flange region is at the 2nd highest hardness value. The flange region is the region with the lowest hardness value. This occurs because various parts of the section are subjected to cooling and tempering at different rates during the cooling process and during the self-tempering process. In addition, the differences in the wall thickness of the web, web+flange and flange regions of the section cause such different hardness values. The cooling rate variation obtained depending on the wall thickness is given in Fig. 6. For the HEA120 section, when the hardness values of the web, web+flange and flange regions are compared (Fig. 16a-c) for 12 bar 30 s cooling process, the web region hardness value is 195 HB as shown in Fig. 9a, and the hardness value of the web region shown in Fig. 9b. The web+flange hardness value is 179 HB and the flange region hardness value shown in Fig. 9c is 140 HB. This type of behaviour in the stiffness of the section regions occurs in an analogous manner in HEB120, as can be seen from Fig. 16.

As can be seen from dimensions of the sections given in TABLE 1, the wall thickness of the web regions is thinner than the other regions. For this reason, it is expected that the web region cools faster, and its hardness is higher than other regions. In addition, in terms of the tensile strength and impact energy, it may be beneficial in practice for some constructions, that the flange region is lower in hardness than other regions. In terms of impact loading, the risk of crack formation and brittle fracture is reduced. Due to the application, the maximum tensile stresses usually occur in the flange region. For this reason, it is helpful in terms of impact loading that the flange region is tough compared to the other regions.

The experimental results of the hardness values of the regions in all examined sections with the cooling rate are given in Fig. 17. The cooling parameters for 12 bar 30 s, 4 bar 10 s and 4 bar 30 s and the hardness changes of the web, web+flange and flange regions of the HEA120 and HEB120 section depending on the cooling rate are shown with different symbols. The hardness values, H related to the cooling rate C_R is derived (Eq. (2)) from the experimental data in Fig. 17.

$$H = 100\, C_R^{0.16} \tag{2}$$

Eq. (2) expressed by evaluating the experimental test results shows that, change in the hardness according to the cooling rate is non-linear. The hardness increases rapidly up to 23°C/s depending on the cooling rate, as seen from the curve in Fig. 17. The increase rate in the hardness decreases considerably at the values above the cooling rate of 23°C/s. Moreover, the curve approaches the limit at high cooling rates. Therefore, values approximately at 100°C/s cooling rate have less effect on hardness. While hardness result is 179 HB at a cooling rate of 23°C/s, it is 195 HB at a cooling rate of 83°C/s.

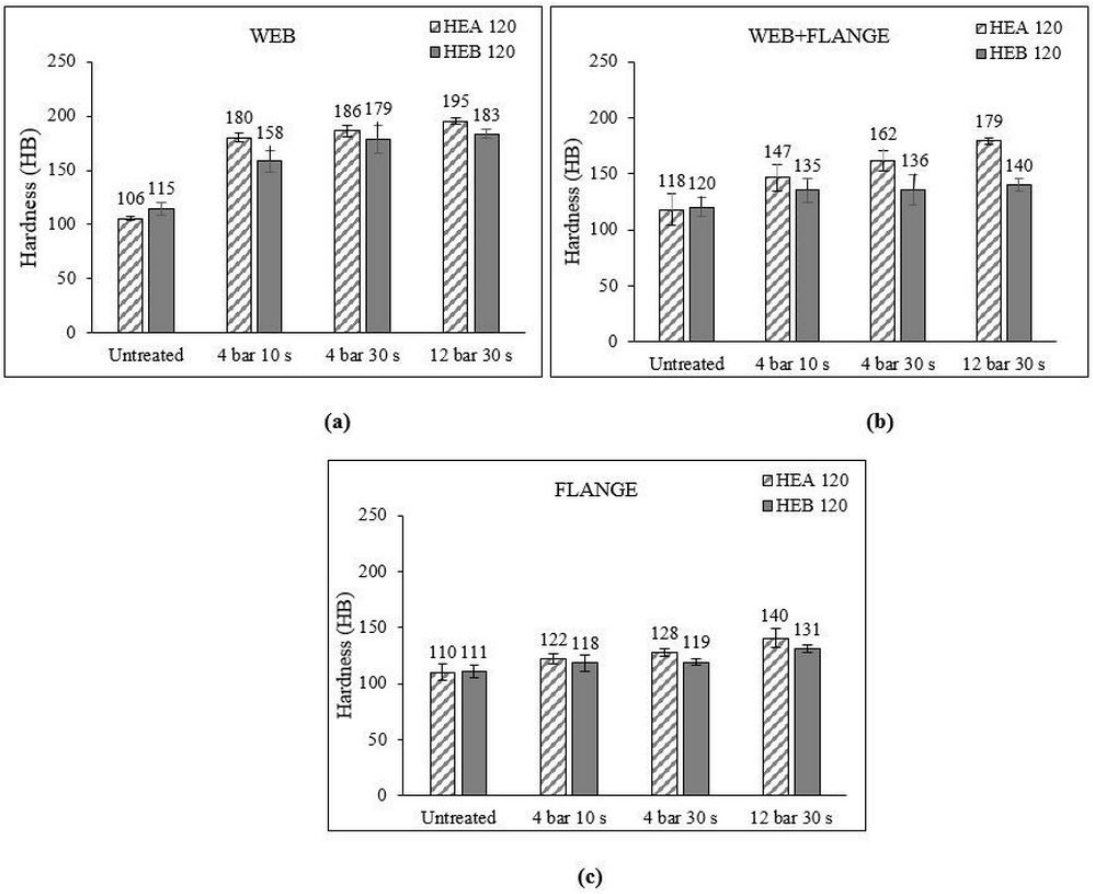

Fig. 16. Variation of the hardness in the a) web, b) web+flange and c) flange regions of the AC-ST HEA120 and HEB120 sections for different parameters (pressure and cooling time)

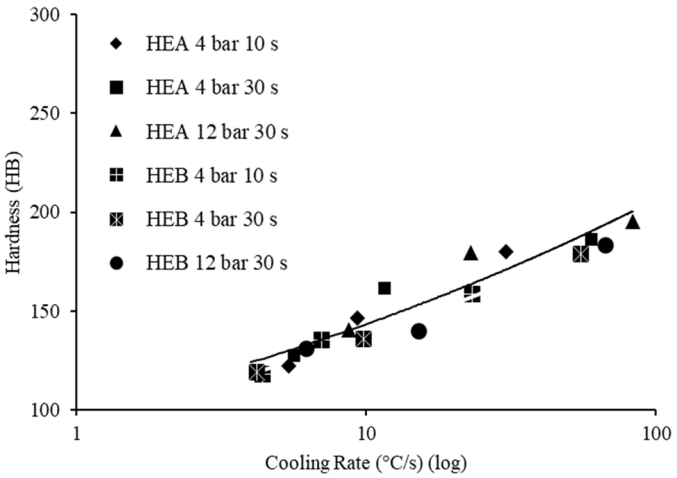

Fig. 17. Hardness versus cooling rate in the web, web+flange and flange regions of the AC-ST HEA120 and HEB120 sections for different parameters (pressure and cooling time)

3.3. Residual Stress

The strain versus time graphs obtained with the cutting (sectioning) method applied to the sections are presented in Fig. 18. Strain in the web and flange regions of the AC-ST sections is compression tensile respectively. The types of the strains in the web and flange regions of the untreated sections are the same as types of the strains in that of the AC-ST sections, with an average of 0.004. While the highest average compression strain in the web region of the AC-ST applied sections was observed as 0.019 for 4 bar 10 s parameter in AC-ST HEB120 section, the average highest tensile strain was exhibited as 0.025 in AC-ST HEA120 section for 4 bar 30 s parameter.

The residual stress values were calculated according to Hooke's law by using the average strain data in Fig. 19. In the web region of the untreated HEA120 section the residual stress is measured as 53 MPa (compressive), while in the flange region there was only tensile stress and the results of it is 39 MPa. In Fig. 19, it has been determined that the compressive residual stress value decreases as the cooling rate increases in the web region. The minimum compressive residual stress value of 283 MPa was obtained at the highest cooling rate (83°C/s) in the web region of the AC-ST HEA120 section. The residual tensile stresses in the flange regions of the examined sections increase as the cooling rate increases, and the extreme residual tensile stress was observed in the HEA120 section at a cooling rate of 6°C/s as 442 MPa.

Spoorenberg et. al. studied the residual stress measurement of the steel sections by shearing method after QST, it was found that there are compressive stresses in the web region of the sections and tensile stresses in the flange regions [14] in accordance

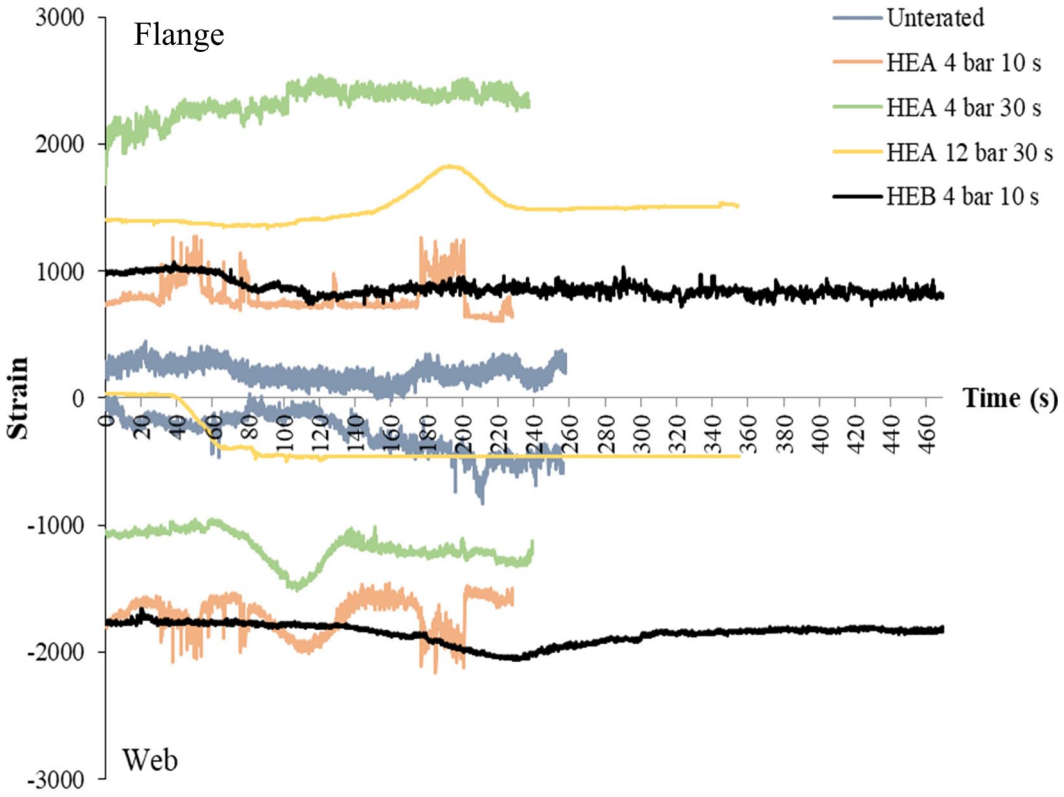

Fig. 18. Strain versus time in the web and flange regions of the HEA120 and HEB120 sections for different parameters (pressure and cooling time)

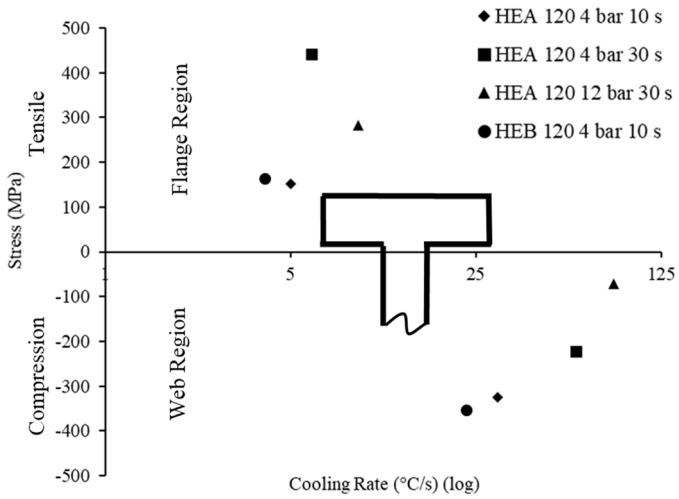

Fig. 19. Residual stress versus cooling rate in the web and flange regions of the HEA120 and HEB120 sections for different parameters (pressure and cooling time)

with this study. Spoorenberg et al. [14] reported that the residual stress is (-)220 MPa (compressive) in the web region and it is 160 MPa (tensile) in the flange region as a result of the QST treatment applied to HISTAR steel. In this study, higher residual values were obtained in terms of both compressive residual and tensile residual stresses due to the AC-ST process carried out with compressed water+air and the thinner wall thickness of the investigated sections. The compressive residual stress was observed as (-)352 MPa in the web region of the AC-ST HEB120 section at a cooling rate of 23°C/s. However, considering the extreme tensile residual stress of 442 MPa determined in the HEA120 section for 4 bar 30 s, it is considered that the yield strength of the given section can be approached. The yield strength of the HEA120 section after AC-ST at a cooling rate of 6°C/s is expected to be 460 MPa empirically by using hardness value [34]. For this reason, the given section did not deform.

4. Conclusions

In this study, AC-ST heat treatment was applied to HEA120 and HEB120 sections for the first time by pulverizing the water+air mixture, at a cooling time of 10 and 30 s with different compressed air values for 4 and 12 bar. The results obtained from the characterization studies are summarized below:

- The highest cooling rate in the web region of the AC-ST HEA120 section for 12 bar 30 s was obtained as 83°C/s. The lowest cooling rate of 4°C/s was obtained in the flange region of the HEB120 section for 4 bar 10 s. As the air pressure applied during the AC-ST process and the cooling time increased (12 bar 30 s), the cooling rate increased. Since the wall thickness of the AC-ST HEA120 section is thinner than that of the AC-ST HEB120 section the cooling rates obtained in web, web+flange and flange regions are greater.
- Ferrite+Pearlite microstructure was observed in the untreated HEA120 and HEB120 sections. In the web region of the AC-ST HEA120 section lower bainite and/or small amount of martensite phases were witnessed at cooling rates of 83°C/s and 60°C/s. When the cooling rate is decreased to

30°C/s, sorbite and/or upper bainite microstructure, as well as acicular ferrite and/or polygonal ferrite microstructure, are seen in the web. For the lowest cooling rate of 4°C/s, acicular ferrite and polygonal ferrite phases were detected in the web+flange and flange regions.

- After the cooling process with the highest cooling rate of 83°C/s, the hardness increase values in the web region were 83% for HEA120 and 59% for HEB120. While the hardness increase values in the flange region of the sections were 27% for HEA120, it was 18% for HEB120. According to these results, the hardness increase of the HEA120 size sections is higher than HEB120 size sections due to thinner wall thicknesses for the same cooling parameters conditions.
- The maximum compressive residual stress of (-)352 MPa in the web region of the AC-ST HEB120 section at a cooling rate of 23°C/s and the extreme tensile residual stress of 442 MPa in the flange region of the AC-ST HEA120 section for a cooling rate of 6°C/s are measured.

Acknowledgment

The authors would like to thank Karabuk University for supporting the preliminary studies with the BAP project coded KBÜBAP-22-KP-084, and the Scientific and Technological Research Council of Turkey for supporting the design/manufacturing of the system with the Tübitak1005 project coded 222M441.

REFERENCES

[1] L. Weber, L.G. Cajot, K. Yemez, Su verilmiş ve kendiliğinden temperlenmiş sıcak haddelenmiş H profillerin kullanımındaki son gelişmeler, Türkiye Mühendislik Haberleri **436** (2), 80-87 (2005).

[2] R. Zanon, G. Axmann, J.C. Gerardy, A. Plumier, The use of heavy rolled sections in High-rise buildings: Current practice and future Innovation, in: Constru Metal 2012, ABCEM, Sao Paulo 2012.

[3] S. Finnigan, B. Charnish, R. Chmielowski, Steel and the skyscraper city: A study on the influence of steel on the design of tall buildings, Council on Tall Buildings and Urban Habitat Research Paper, 114-123 (2015).

[4] https://sections.arcelormittal.com/repository2/Sections/1_HISTAR_High%20Strength/5_01_24_Histar_ASTM_A913_seismic_ncee_en.pdf

[5] A. Fujibayashi, K. Omata, JFE Steel's advanced manufacturing technologies for high performance steel plates, JFE Technical Report 5, 10-15 (2005).

[6] L. Weber, Histar high performance hot-rolled beams, Advanced Materials for Construction of Bridges, Buildings, and Other Structures III, Switzerland 2003.

[7] Z. Bo, S. Yong, L. Tan, H.X. Yang, W.Q. Cao, Y.Z. Bao, Research on a new process of the non-quenched and tempered steel with high strength and high toughness, Physics Procedia **50**, 25-31 (2013). DOI: https://doi.org/10.1016/j.phpro.2013.11.006

[8] J. Hoffmann, B. Donnay, TMCP applications in sections, bars and rails, Profilarbed Research, Luxembourg 2004.

[9] M. Rocha, E. Brühwiler, A. Nussbaumer, Geometrical and material characterization of quenched and self-tempered steel reinforcement bars, Journal of Materials in Civil Engineering **28**, 04016012 (2016).
DOI: https://doi.org/10.1061/(ASCE)MT.1943-5533.0001355

[10] X. Kong, L. Lan, Optimization of mechanical properties of low carbon bainitic steel using TMCP and accelerated cooling, Procedia Engineering **81**, 114-119 (2014).
DOI: https://doi.org/10.1016/j.proeng.2014.09.136

[11] S. Tang, Z.Y. Liu, G.D. Wang, R.D.K. Misra, Microstructural evolution and mechanical properties of high strength microalloyed steels: Ultra Fast Cooling (UFC) versus Accelerated Cooling (ACC), Materials Science and Engineering A **580**, 257-265 (2013).
DOI: https://doi.org/10.1016/j.msea.2013.05.016

[12] https://sections.arcelormittal.com/repository2/Sections/5_3_1_HISTAR_web.pdf

[13] S. Shinde, M. May, Recent developments in the use of quenched and self-tempered hot rolled H-beams, COMAT 2012 – 2nd International Conference on Recent Trends in Structural Materials, Czech Republic 2012.

[14] R.C. Spoorenberg, H.H. Snijder, L.G. Cajot, M.S. May, Experimental investigation on residual stresses in heavy wide flange QST steel sections, Journal of Constructional Steel Research **89**, 63-74 (2013).
DOI: https://doi.org/10.1016/j.jcsr.2013.06.009

[15] S.H. Jung, M.S. Yun, B.S. Koo, K.K. Lee, Influence of non-uniform water cooling on the shape of rolled H-shaped beam, 145th TMS Annual Meeting & Exhibition, Nashville Tennessee 2016.

[16] B.S. Koo, Longitudinal bending behaviors of hot-rolled H-beams by quenching and self-tempering, Engineering Failure Analysis **133**, 106009 (2022).
DOI: https://doi.org/10.1016/j.engfailanal.2021.106009

[17] H. Zengin, H. Ahlatci, S. Oner, M.E. Demirkazik, S. Ozcelik, Y. Turen, Y. Sun, The effect of accelerated cooling on microstructure and impact strength of S355J2 quality steels used in power transmission line construction, Universal Journal of Materials Science **7** (1), 1-5 (2019).
DOI: https://doi.org/10.13189/ujms.2018.070101

[18] H.H. Snijder, L.G. Cajot, N. Popa, R.C. Spoorenberg, Buckling Curves for Heavy Wide Flange Steel Columns, Rev. Roum. Sci. Tech., Méc. Appl., Tome 55, Nº, P., Bucarest, 2010.

[19] https://www.researchgate.net/post/How-to-decide-holding-time-for-any-heat-treatment

[20] https://www.voestalpine.com/highperformancemetals/international/en/service/heat-treatment/

[21] Commission of the European Communities, Technical Steel Research, Quenching and self-tempering (QST) of beams in the rolling heat, Luxembourg, 1992.

[22] B.S. Koo, A theoretical approach for estimating the effect of water-jet quenching on low-carbon steel beams, Scientific Reports **11**, 15401 (2021).
DOI: https://doi.org/10.1038/s41598-021-03591-3

[23] G. Krauss, S.W. Thompson, Ferritic Microstructures in Continuously Cooled Low- and Ultralow-carbon Steels, ISIJ International **35**, 937-945 (1995).
DOI: https://doi.org/10.2355/isijinternational.35.937

[24] P.C.M. Rodrigues, E.V. Pereloma, D.B. Santos, Mechanical properities of an HSLA bainitic steel subjected to controlled rolling with accelerated cooling, Materials Science and Engineering A **283** (8), 136-143 (2000).
DOI: https://doi.org/10.1016/S0921-5093(99)00795-9

[25] A. Das, S. Sunil, R. Kapoor, Effect of cooling rate on the microstructure of a pressure vessel steel, Metallography, Microstructure, and Analysis **8**, 795-805 (2019).
DOI: https://doi.org/10.1007/s13632-019-00585-6

[26] D. Rasouli, Sh.K. Asl, A. Akbarzadeh, G.H. Daneshi, Effect of cooling rate on the microstructure and mechanical properties of microalloyed forging steel, Journal of Materials Processing Technology **206**, 92-98 (2008).
DOI: https://doi.org/10.1016/j.jmatprotec.2007.12.006

[27] Z.X. Li, B.Q. Tong, Q.L. Zhang, J.H. Yao, V. Kovalenko, Z.G. Li, Influence of initial microstructure on the microstructure evolution and mechanical properties of 1.0C-1.5Cr steel in the laser surface quenching, Materials Science and Engineering A **788**, 139490 (2020). DOI: https://doi.org/10.1016/j.msea.2020.139490

[28] Y. Sun, J. Chen, J. Liu, Effect of hydrogen on ductility of high strength quenched and tempered (QT) Cr-Ni-Mo steels, Materials Science and Engineering A **625**, 89-97 (2015).
DOI: https://doi.org/10.1016/j.msea.2014.12.013

[29] C.P. Liu, J.Z. Pan, P.T. Liu, R.M. Ren, X.J. Zhao, Influence of original microstructure on rolling contact fatigue property of D2 wheel steel, Wear, 203380 456-457 (2020).
DOI: https://doi.org/10.1016/j.wear.2020.203380

[30] https://www.quora.com/How-is-bainite-formed-and-also-what-are-upper-bainite-and-lower-bainite

[31] H.K.D.H. Bhadeshia, J.W. Christian, Bainite in steels, Metallurgical Transactions A **21**, 767-797. (1990).
DOI: https://doi.org/10.1007/BF02656561

[32] A.B. Cota, D.B. Santos, Microstructural characterization of bainitic steel submitted to torsion testing and interrupted accelerated cooling, Materials Characterization **44**, 291-299 (2000).
DOI: https://doi.org/10.1016/S1044-5803(99)00060-1

[33] H. Ohtani, S. Okaguchi, Y. Fujishiro, Y. Ohmori, Morphology and properties of low-carbon bainite, Metallurgical Transactions A **21**, 877-888 (1990).
DOI: https://doi.org/10.1007/BF02656571

[34] W.D. Callister, D.G. Rethwisch, Materials Science and Engineering An Introduction, 2009 Wiley, USA.